Project Report 20155: Remote Mapping of Surface Ruptures of the 2019 Ridgecrest Earthquakes

Summary

We used post-earthquake lidar data and other imagery to remotely map surface ruptures and measure offsets produced by the 2019 Ridgecrest Earthquake sequence, independent of observations collected in the field. The 4 July MW 6.4 and 5 July MW 7.1 earthquakes produced surface rupture zones approximately 20 km and 50 km in length, respectively, that span up to four kilometers in width, with numerous surficial fractures occurring more than 10 km from the main rupture. The purpose of this study is to develop an objective, uniform map product from which we test 1) the reproducibility of remote surface-rupture mapping and slip measurements between individual remote mappers and 2) the accuracy of remote compared to field-derived surface-rupture mapping and slip measurements. The first phase of this project is remote mapping of the surface rupture by three independent mappers with various backgrounds in active tectonics. This mapping is done from the post-earthquake airborne lidar and imagery data, without input from post-earthquake field mapping. Visual comparison of the three remote rupture maps show good agreement for scarps > 50 cm. For features with less topographic expression, interpretations of the data vary more widely between mappers. Quantitative comparisons range from 40 to 80% consistency between maps. In general, field observations and airborne imagery detect more surface rupture features than airborne lidar. Lidar excels for detection and measurement of vertical offsets in the landscape.

Intellectual Merit

Earthquake surface-rupture mapping provides essential data for seismic hazard evaluation and for understanding earthquake physics. Detailed geomorphic features of surface ruptures decay rapidly, requiring rapid field response to capture perishable data. As a result, few parts of a rupture are visited by more than one field team, leading to variable mapping detail and little to no information on the reproducibility of measured offsets. For the Ridgecrest Earthquake Sequence, we use post-earthquake lidar and imagery surveys to interpret and map the surface rupture. We compare results from multiple skilled mappers, and with independently collected field measurements, to objectively analyze the reproducibility of post-event maps.

Broader Impacts

This work will provide essential data for probabilistic fault displacement hazard assessments (PFDHA). This project provided summer research support and salary to UC Davis graduate students Alba M Rodriguez Padilla and Elaine K Young; was used as a teaching exercise and a graduate course on active tectonics during which course participants mapped a small part of the rupture using only the lidar data; and facilitated and remote mapping experience to replace field course work for two graduating seniors (Sergio Mendoza and Kimberly Bowman) during Covid-19 shutdowns. Preliminary results from this project were presented at the 2020 SCEC annual meeting and final results in analyses will be distributed in one research publication.

Technical Report

The primary goal of this proposal is to produce a map of the 2019 Ridgecrest sequence surface rupture generated by three independent mappers exclusively from lidar and other remotely sensed data. Using this map product to test the reproducibility of remote rupture maps and to compare with pre-event mapping and field-based mapping to further our understanding of fault ruptures locations. The large area covered by airborne lidar to document the 2019 Ridgecrest earthquake sequence allows for detailed remote mapping covering regions far from the principal rupture trace. Understanding the quality and reproducibility of surface rupture maps covering these areas is important for guiding future field efforts in response to major earthquakes.

To begin, each of the three mappers set up a project and GIS using the 2019 Ridgecrest lidar data. A variety of visualizations were used to view the topography. These visualizations included dynamically scaled elevation color ramps, slope shades, high-pass filtered elevations, and hillshade images with variable sun orientations and vertical exaggeration. We started with a 13 km section of the M7.1 rupture centered on the China Lake Naval base. Once all three mappers completely mapped that area we assessed the amount of overlap between each of the different maps.

To assess percent overlap in rupture maps we first converted the vector/shape files to 1 m rasters. We also created a raster for each mapper that had an additional 1 m buffer on either side. This rasterization removes variability in line length and allows for subtle variations in line placement when mapping the same feature. Rasterization also removes the continuity of lines when mapping a single feature from the analysis, allowing us to focus exclusively on comparing whether or not a feature was mapped in that location. We calculate the amount of pixel overlap between a primary rastererized map and secondary rasterized map with buffer. The number of shared pixels divided by the total number of pixels in the primary map yields the percent overlap. For the initial area we mapped, our individual maps tend to agree with each other between 40% and 80%. Map disagreement depends largely on the number and location of ruptures mapped, rather than differences in mapping of the same features. In other words, location accuracy is good but interpretation of what features constitute rupture varies. When compared with rupture maps compiled using field data, the differences in location of lines mapped is often a function of what is visible in the field versus in the lidar. Field observations detect scarps that are shorter than can be discriminated from laser altimetry, as well as small fissures and cracks without vertical offset. Such features would be missed by our mapping efforts.

Currently, we have completed rupture mapping for the entire lidar data set, and analysis of these maps is ongoing. We are conducting parallel mapping efforts using drone- and aircraft-collected photography. We find that the number and extent of fault ruptures evident in these data greatly exceeds that detectable from the lidar data.

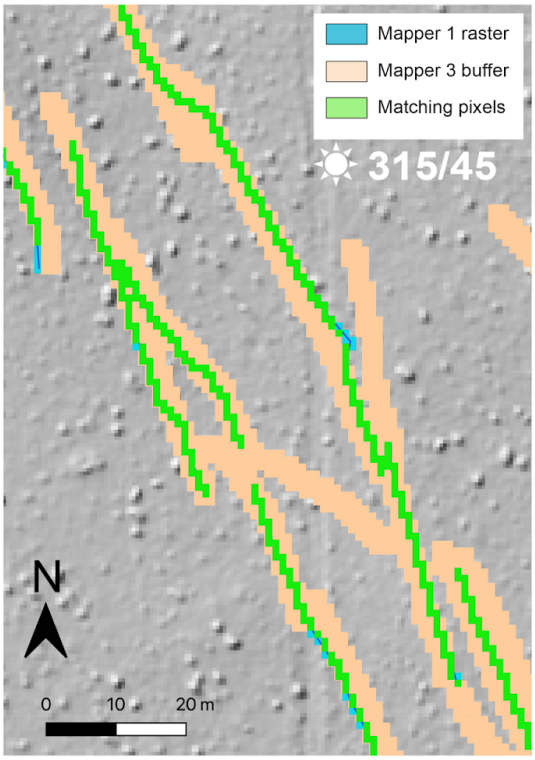

Figure 1. Comparison of rasterized rupture maps. Mapper 1 lines converted to one meter pixels and compared against mapper 3 lines converted to 1 meter pixels with a 1 m buffer zone. Most of mapper 1 lines lie within the buffered region (green pixels); a few lines fall slightly outside of these buffered zones (blue pixels).

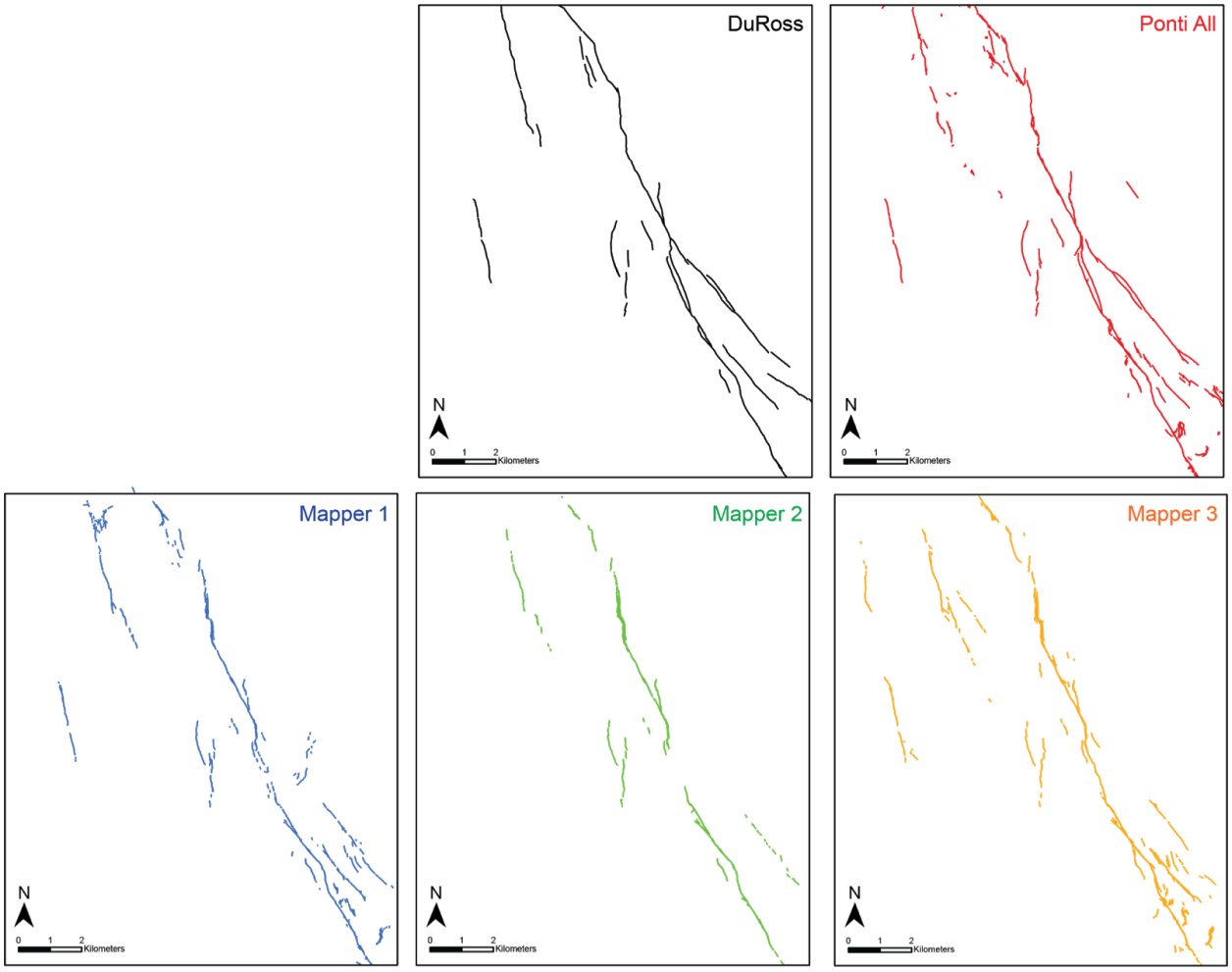

Figure 2. Comparison of two field-mapping products (DuRoss et al., 2020 and Ponti et al., 2020) with three independently produced lidar-derived maps of a 13 km section of the M7.1 Ridgecrest earthquake surface rupture.

Percent Overlap Between Mappers

Compared to	Mapper 1	Mapper 2	Mapper 3	DuRoss	Ponti Field	Ponti All
Mapper 1	100	60	41	16	28	23
Mapper 2	52	100	44	18	31	24
Mapper 3	67	80	100	23	40	32
DuRoss	19	22	16	100	17	20
Ponti Field	18	25	16	10	100	44
Ponti All	36	44	31	27	100	100
Ponti All 2m	47	58	42	42	100	100

How we got those numbers

Sum of (*Mapper 1 raster* * *Ponti All 2m buffer raster*) / Sum of *Mapper 1 raster* * 100 = 20,329 / 42,915 * 100 = 47%

So...
47 % of Mapper 1's lines are within 2 m of Ponti All lines
53 % of Mapper 1's lines are not within 2 m of Ponti All lines

Figure 3. Grid of comparisons of map products. Primary maps (columns) compared against secondary maps with buffers (rows). Ponti All includes lines derived from remote-sensing observations in addition to field observations.

References

DuRoss, C. B. et al., 2020, Surface Displacement Distributions for the July 2019 Ridgecrest, California, Earthquake Ruptures, Bulletin of the Seismological Society of America, 110, no. 4, 1400–1418, doi: 10.1785/0120200058.

Ponti, D. J. et al., 2020, Documentation of Surface Fault Rupture and Ground-Deformation Features Produced by the 4 and 5 July 2019 Mw 6.4 and Mw 7.1 Ridgecrest Earthquake Sequence, Seismological Research Letters, 91, no. 5, 2942–2959, doi: 10.1785/0220190322.